NARROW LINE REGION PROPERTIES

1.1 INTRODUCTION

Correlations between the masses of super-massive black holes and properties of the host galaxy bulges in nearby galaxies (Gebhardt et al., 2000; Ferrarese and Merritt, 2000) and the similarity of the cosmic evolution of star formation and black hole activity (Boyle and Terlevich, 1998; Madau and Dickinson, 2014) suggest that the formation and evolution of supermassive black holes and their host galaxies are linked. Active galactic nuclei (AGN) and quasar feedback, in which star formation in the host galaxy is supressed by the energy output from the quasar, is a favoured model. This has motivated a considerable amount of observational work searching for feedback signatures (for recent reviews, see Alexander and Hickox, 2012; Fabian, 2012; Heckman and Best, 2014).

The [O III]$\lambda\lambda$4960,5008 doublet is the strongest narrow line found in optical quasar spectra. It is forbidden line which traces gas on kiloparsec scales. High velocity dispersions or strong asymmetries in forbidden lines are evidence of high velocity extended ionized outflows. Recent studies have provided constraints on the prevalence of ionized outflows traced by [O III] emission in low-redshift type 2 AGN (e.g. Mullaney et al., 2013; Zakamska and Greene, 2014) using spectra from the Sloan Digital Sky Survey (SDSS; York et al., 2000). However, the signatures of feedback are expected to be stronger at higher redshifts ($z \sim 2$) when the black hole accretion and star formation rates both peak.

In this paper we analyse the [O III] properties of a sample of 358 high-luminosity, redshift $1.5 < z < 4$ quasars. In particular, we search for signs of outflowing gas, which include assymetries and broad velocity widths. Recent near-IR spectroscopy of $z > 1.5$ quasars often report exceptionally large [O III] widths, with FWHM $> 1000 \mathrm{km\,s}^{-1}$(e.g. Netzer et al., 2004; Nesvadba et al., 2008; Kim et al., 2013; Brusa et al., 2015; Carniani et al., 2015; Perna et al., 2015). **Add reference to WIISH paper**.

To date, the focus has been extreme, rare, AGN sub-populations, e.g. highly reddened and obscured AGN (Banerji et al. 2012,2013,2014, Eisenhardt et al. 2012, Ross et al. 2014, Zakamska et al. 2016, WIISH paper). These populations provide insight into relatively short-lived phases in the AGN activity cycle. A more complete understanding of AGN-evolution and the physical link with the host galaxies requires
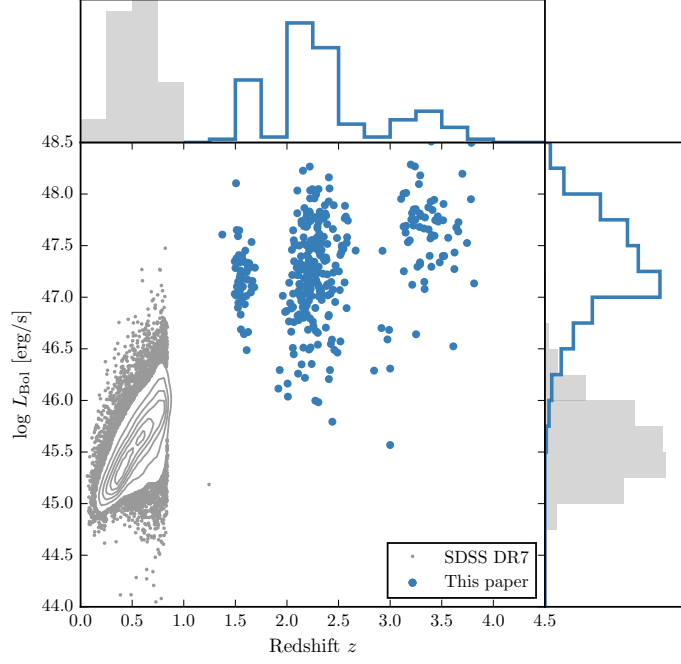
Figure 1.1: The ranges in redshift and luminosity covered by our sample, relative to the redshift-luminosity distribution of the SDSS DR7 quasar catalogue with measured [O III] line properties (Shen et al., 2011). The gaps in our sample coverage at $z \sim 1.8$ and $z \sim 3$ are due to the near-infrared transmission windows. In regions of high point-density, contours show equally-spaced lines of constant probability density generated using a Gaussian kernel-density estimator.

the rare, extreme, sub-populations to be placed in the context of the AGN population as a whole.

For a subsample where we have spectra covering the rest-frame ultra-violet line C IV, we can test whether the strong outflows, inferred the blueshifting of C IV relative to the systemic redshift, have any effect on the host galaxy on larger scales.

Throughout this paper we adopt a flat ΛCDM cosmology with $h_0 = 0.69$ and $\Omega_M = 0.29$.

The paper is structured as follows.

1.2 QUASAR SAMPLE

We have assembled a catalogue of 358 high-luminosity, redshift $1.5 < z < 4$ quasars, with spectra taken in the near-infrared. At these redshifts the spectra cover the rest-frame optical region, which includes the broad Balmer Hβ line and the strong, narrow [O III] doublet. There is a significant overlap between the sample presented here and the one used in Coatman et al. (2016b), hereafter paper I. We briefly

describe the catalogue below, but refer the reader to Coatman et al. (2016b) for further details, including the reduction procedure.

Two hundred are selected from the SDSS Seventh Data Release (DR7; Schneider et al., 2010). These are observed with LIRIS (Manchado et al., 1998) on the William Herschel Telescope (WHT), TripleSpec (Wilson et al., 2004) on the Astrophysics Research Consortium (ARC) 3.5 m telescope, FIRE (Simcoe et al., 2010) on the Magellan-Baade telescope, the SINFONI integral field spectrograph (Eisenhauer et al., 2003; Bonnet et al., 2004) on the European Southern Observatory (ESO) Very Large Telescope (VLT), SOFI (Moorwood, Cuby, and Lidman, 1998) on the New Technology Telescope (NTT), and TRIPLE-SPEC on the Palomar 200-inch Hale telescope (P200). One hundred and seventeen were observed to measure accurate redshifts of quasar pairs at very close projected separations (Prochaska and Hennawi, 2009; Lau, Prochaska, and Hennawi, 2015; Hennawi et al., 2015). Spectra were taken with GNIRS (Elias et al., 2006) on the Gemini North telescope, ISAAC (Moorwood et al., 1998) on the European Southern Observatory (ESO) Very Large Telescope (VLT), NIRSPEC (McLean et al., 1998) on the Keck-II telescope, NIRI (Hodapp et al., 2003) also on Gemini North, and XSHOOTER (Vernet et al., 2011), again, on the VLT. Seventy-nine are bright Hamburg-ESO quasars observed with SINFONI, ninety are quasars with archival high-resolution optical spectra observed with SOFI, and four are observed with XSHOOTER and presented in the XQ-100 catalogue (Lopez et al., 2016).

This is the largest study of the narrow line region properties of high-z quasars ever undertaken. The redshift and luminosity coverage of the quasars in our sample is shown in Fig. 1.1, and the quasar sample is summarised in Table 1.1. Our sample covers much higher redshifts and luminosities than the SDSS sample.

1.3 PARAMETERIC MODEL FITS

In this section we describe how we measure the [O III] velocity-width and parameterize asymmeteries in the line. We first fit a parameteric model to the [O III] emission, and the nearby Hβ peak. This step is taken soley to enhance the signal-to-noise (SNR) of the spectra and to decompose the emission from Hβ and the [O III] doublet. We then calculate non-parameteric measures of the line profile from the best-fitting model.

Before the model can be fit, the spectra must first be transformed in to the (approximate) quasar rest-frame. This transformation is only for practical purposes and the emission line parameters we will go on to derive are independent of the exact redshift used. The redshift will later be refined using the results from the fit. The redshift used in this transformation is either derived from a multi-component Gaussian fit to the broad Hα emission (∼ 40 per cent of our sample) or, when this

Table 1.1: The numbers of quasars with [O III] line measurements and the spectrographs and telescopes used to obtain the near-infrared spectra. Further details on the instrumental configurations are given in paper I. **Check numbers.**

Spectrograph	Telescope	Number
FIRE	MAGELLAN	32
GNIRS	GEMINI-N	29
ISAAC	VLT	8
LIRIS	WHT	5
NIRI	GEMINI-N	29
NIRSPEC	Keck II	3
SINFONI	VLT	76
SOFI	NTT	78
TRIPLESPEC	ARC-3.5m	27
TRIPLESPEC	P200	46
XSHOOTER	VLT	25
		144

is not possible, from a preliminary fit to the broad Hβ emission (~ 40 per cent) or narrow [O III] emission (20 per cent). **Should say whether we use peak/median etc.**

The continuum and optical Fe II emission is modelled and subtracted using a recipee that is identical to the one described in paper I. The following model is then fit to the spectra in the wavelength interval 4700-5100 Å. The fit is done as a function of the Doppler velocity shift, and we adopt the wavelength 4862.721Å (the laboratory Hβ wavelength) to transform wavelengths into equivalent Doppler velocities.

Hβ is modelled by two Gaussians with non-negative amplitudes and FWHM greater than $1200 \mathrm{km\,s}^{-1}$. A handful we fix the centroids of the two Gaussians to be the same, normally because of very low S/N or because the blue wing is below the lower wavelength limit of the spectrograph. Any contribution to the Hβ emission from the narrow-line region is weak in the vast majority of our sample, and so we do not include an additional Gaussian component to model this emission. Note: we do in fact include narrow components for eight objects in our sample. Although, for some objects, this could bias our estimate of the velocity-width of the broad component, this information is not used in the analysis presented in this paper.

Each component of the [O III] doublet is fit with one or two Gaussians, depending on the fractional reduced χ^2 difference between the one- and two-component models. If the addition of the second

Table 1.2: Approximate physical origin of the ICA components.

Component	Origin
w_1	Fe II
w_2	Hβ
w_3	Hβ
w_4	[O III] core
w_5	[O III] core
w_6	[O III] wing

Gaussian decreases the reduced χ^2 by more than 5 per cent then the double-Gaussian model is accepted. One hundred and twenty-five are fit with a single Gaussian, 147 with two Gaussians, and [O III] is undetected in a further 78 quasars. When a single Gaussian is used to model each line, the peak flux ratio of the [O III] 4960 Å and 5008Å components are fixed at the expected 1:3 ratio and the width and velocity offsets are set to be equal. In the double Gaussian fit, the peak flux ratio of the second components is again fixed at 1:3, and the width and velocity offsets are again set to be equal.

In six quasars a significantly better fit was obtained by allowing the flux ratio between the two components to vary. In these quasars the best-fitting peak ratio varies from 0.50 to 0.84, with mean 0.70. **Check ICA component fits to see if this looks real.**

Model parameters were derived using a standard variance-weighted least-squares minimisation procedure employing the Levenberg-Marquardt algorithm. Prior to the fit, the spectra were inspected visually and regions significantly affected by telluric absorption or of low S/N were masked out.

However, the fits aren't always good. How to be quantitative about this? Chi-squared values indicating bad fits? Also the fact that we sometimes model Fe as OIII. Discuss the limitations of using the Boroson & Greene template? Even if don't use results, should discuss Gaussian fits and their limitations, because that's what most people will be using.

1.3.1 *Derived Parameters*

All [O III] line properties are derived from the [O III]5008 emission, but, as described below, the kinematics of the peak at 4960Å are constrained by our fitting routine to be identical.

We do not to attach any physical meaning to the individual Gaussian components used in the model. While it is true that in some quasars the [O III] emission can be clearly separated in to a narrow component at the systemic redshift and a lower-amplitude, blueshifted broad component (e.g. Shen, 2016), often this decompo-
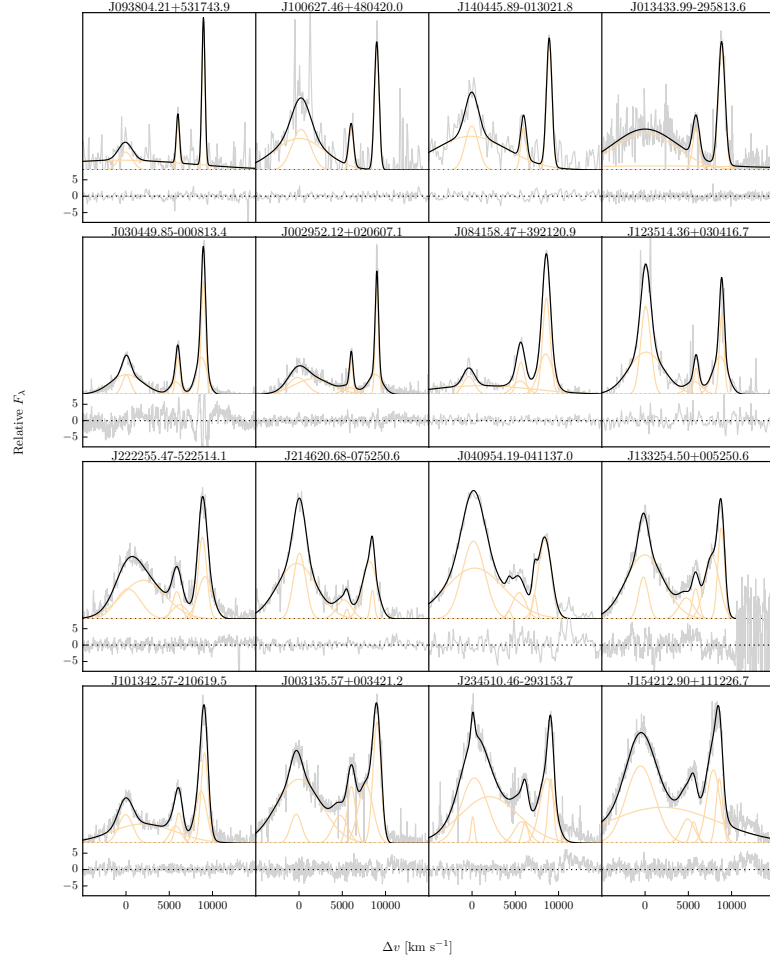
Figure 1.2: Multi-component Gaussian fits to the continuum-subtracted Hβ/[O III] emission in 16 quasars, chosen to be the representative of the wide range of [O III] line widths we measure in our sample. The data is shown in grey, the best-fitting parametric model in black, and the individual model components in orange. The broad Hβ centroid is used to measure the systemic redshift, and Δv is the velocity shift from the line rest-frame transition wavelength for Hβ. Below each fit we plot the data minus model residuals, scaled by the errors on the fluxes. **Resample model at higher resolution.**

$$\frac{w_i}{\sum_{i=1}^{6} w_i}$$
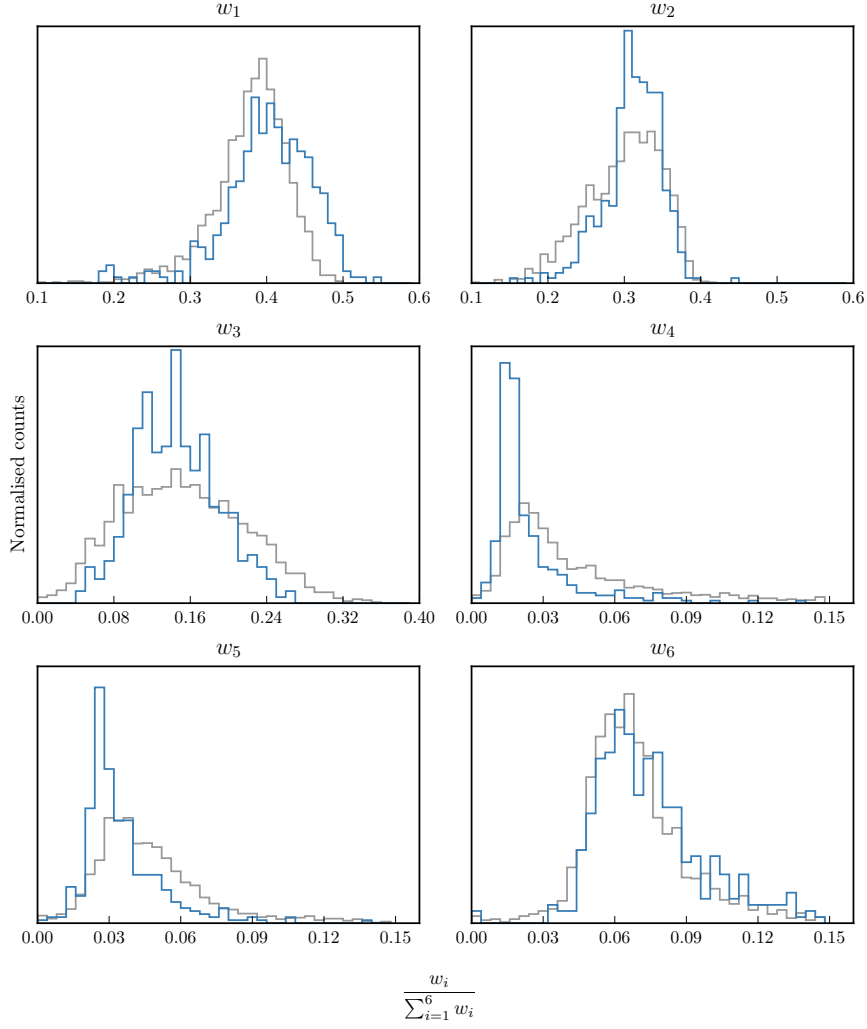
Figure 1.3: The relative weight in each of the six positive ICA components for the high-luminosity (blue) and low luminosity samples (grey). In the high-luminosity sample Fe II emission is stronger (component w_1). The core [O III] emission is weaker (components w_4, w_5) but the strength of the blueshifted wing is the same (w_6).
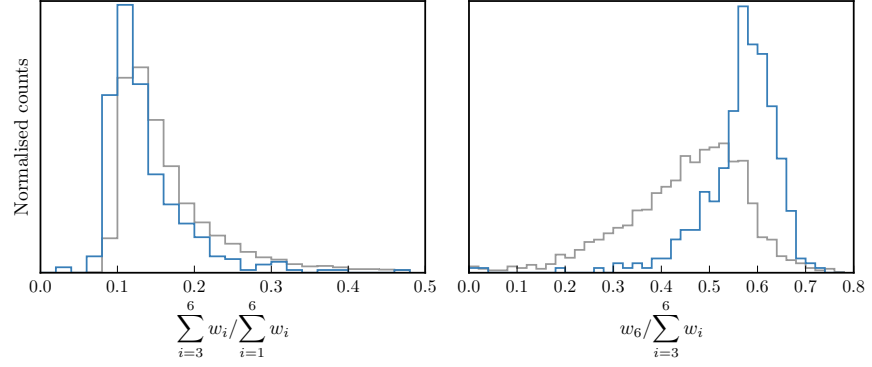
Figure 1.4: The relative weight in the three ICA components corresponding to [O III] emission (*left*) and the relative weight of the component most closely related to blueshifted [O III] emission relative to all three [O III] components (*right*). [O III] emission is weaker in the high-luminosity sample, but the relative contribution but the fractional contribution from the blueshifted component to the total [O III] emission is higher. Hence [O III] is weaker, broader, and more asymmetric in the high-luminosity sample. See Zakamska discussion.
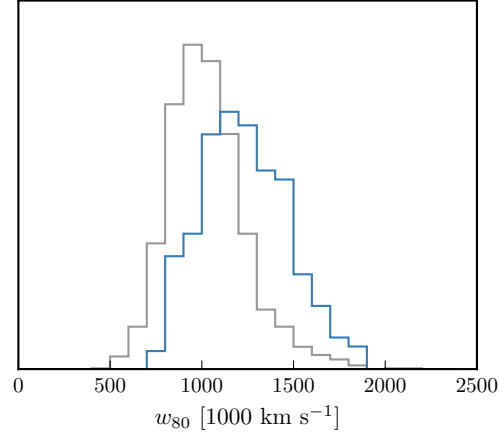
Figure 1.5: Comparison of [O III] velocity-widths in the high and low luminosity samples using the ICA component fits. If keep this need to explain in text how w_{80} is calculated from ICA component fits.
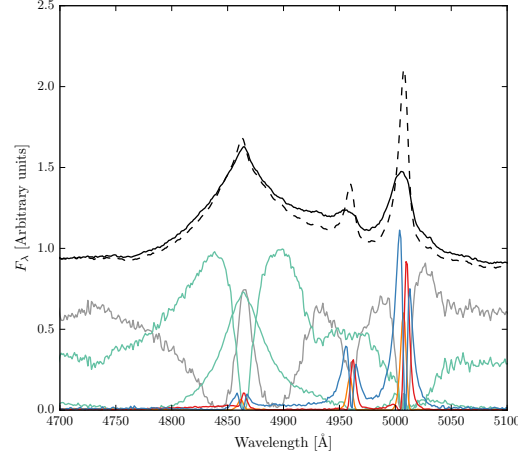
Figure 1.6: Black solid line is the median from the ICA fits to the high-luminosity sample. Black dashed line shows the median from the low-luminosity sample. The six positive ICA components are also shown.
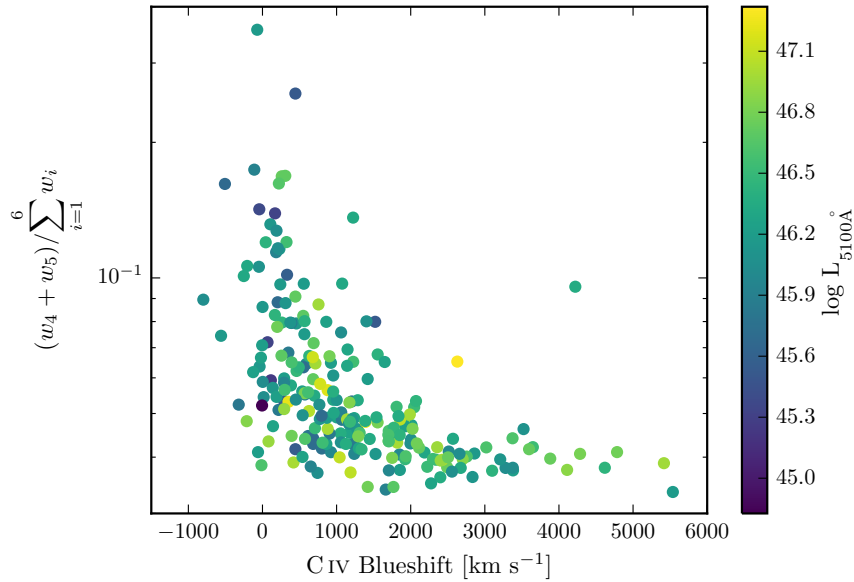

Figure 1.7: [O III] strength decreases as the C IV blueshift increases, I run in to problems comparing the C IV blueshift to the [O III] blueshift / velocity-width. See similar thing if I use [O III] EQW instead. Need to fix y ticks. Only showing the core components here. The C IV blueshift is now measured relative to the NIR ICA redshift. I think this is trend is mostly being driven by the Eigenvector 1 correlations: as the blueshift increases the Fe II strength increases and the [O III] strength decreases. Doesn't appear to be driven by the luminositiy. Is this tighter than EV1 trend shown with Fe/OIII strength by other authors? Is the AGN NLR absent in objects where outflows have reached kiloparsec scales, sweeping up the low-density material responsible for the [OIII]-emission?
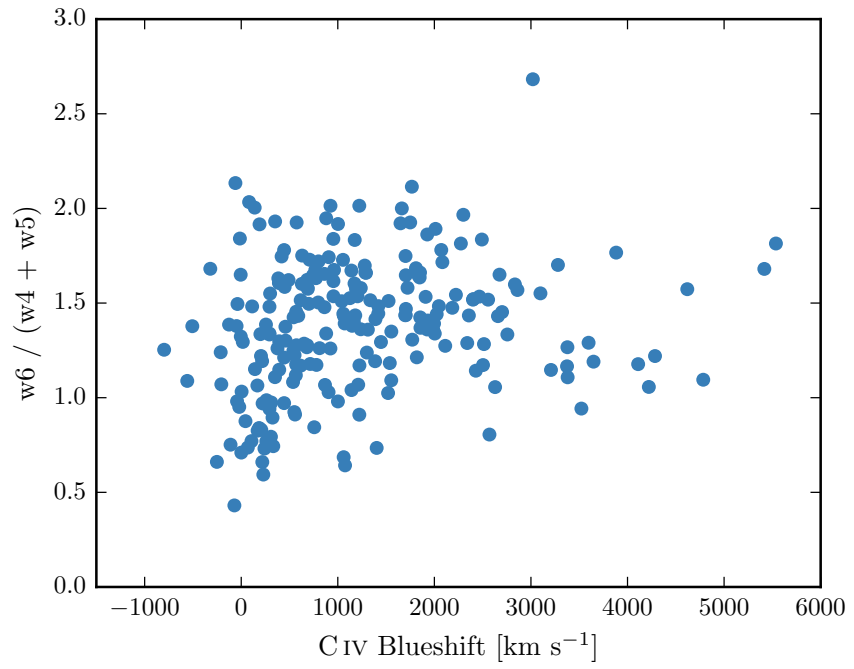
Figure 1.8: I think there is a trend here but at high blueshifts the OIII is undetected / very low S/N. Need to determin when we can believe OIII paramters. Why at low CIV blueshift is there a much bigger dynamic range than in [O III] blueshifts in Fig. 13. Is it just because we have more objects?
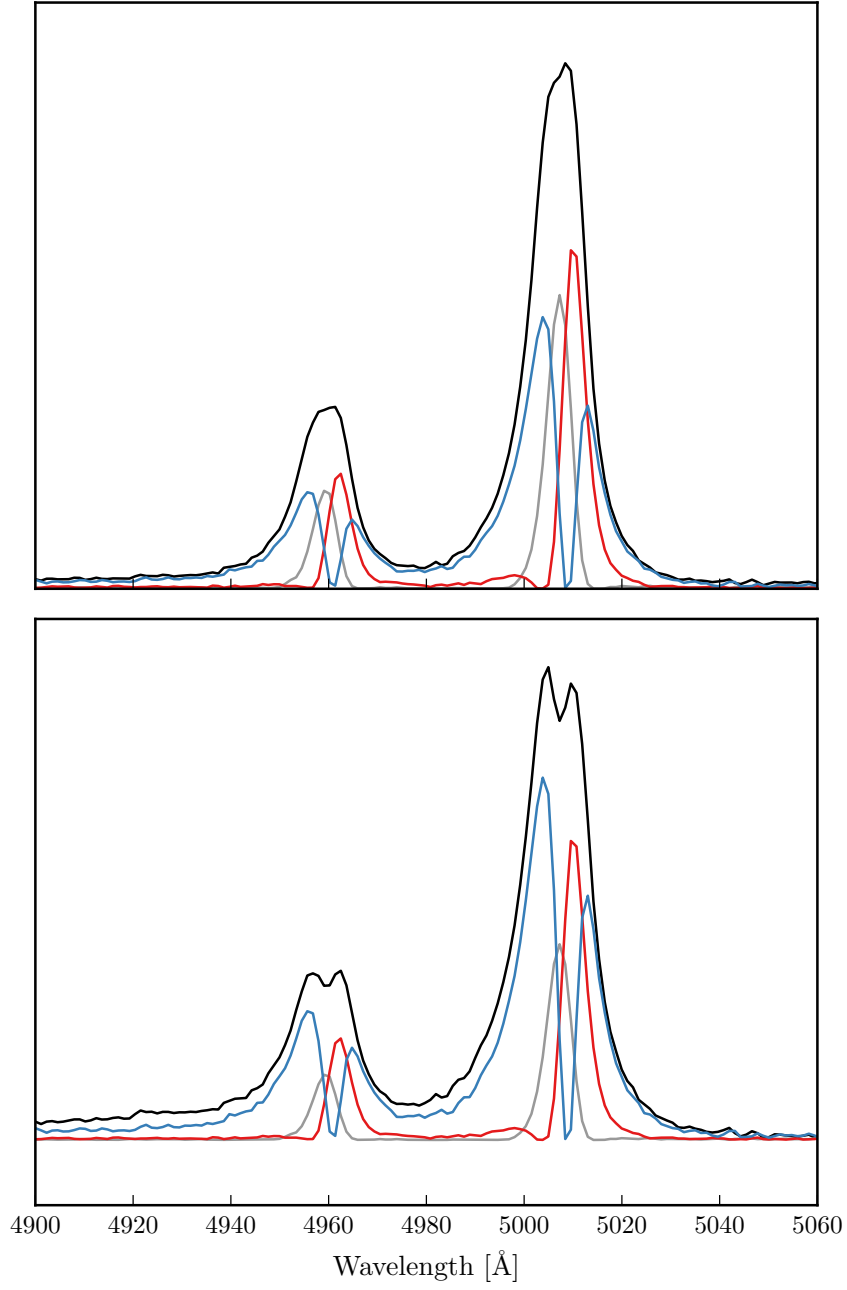
Figure 1.9: Comparison of median [O III] profiles from ICA fits it low- and high-luminosity samples.
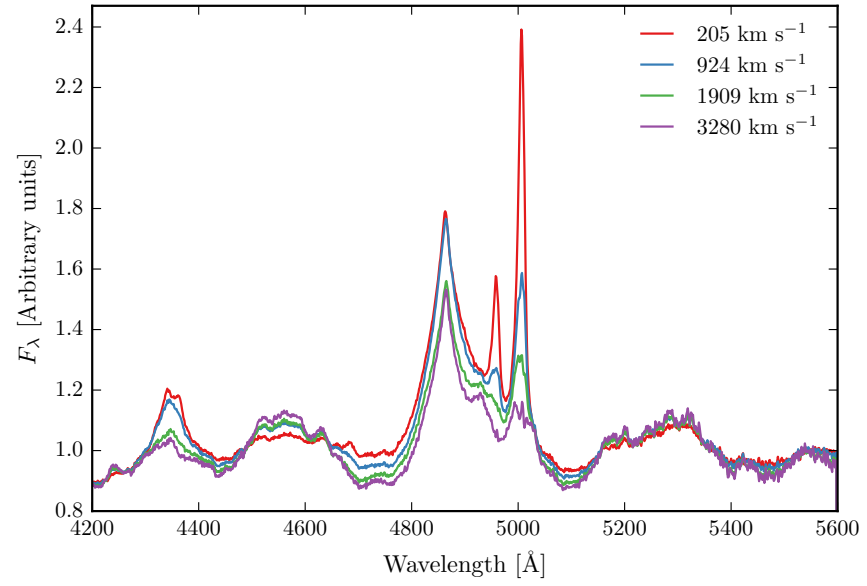
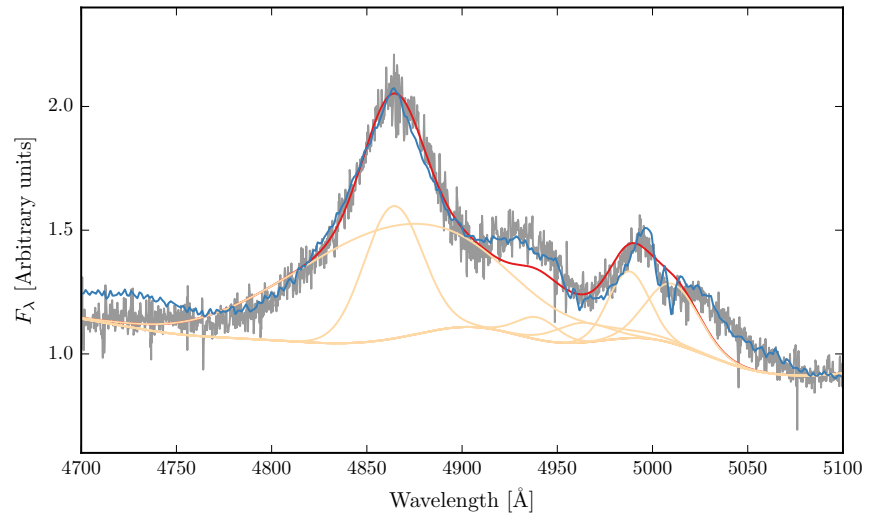Figure 1.10: ICA median weights as a functino of the CIV blueshift.

Figure 1.11: Example where poorly subtracting the iron can be confused with [O III].

sition is highly uncertain. Furthermore, often the S/N is not sufficient to statistically justify the addition of a second Gaussian component. Instead, we characterize the [O III] line profile using a number of non-parameteric measures, which are commonly used in the literature (e.g. Zakamska and Greene, 2014; Zakamska et al., 2016). A normalised cumulative velocity distibution is constructed from the best-fitting model, from which the velocities below which 5, 10, 25, 50, 75, 90, and 95 per cent of the total flux accumulates can be read off. The width of the emission line can then be defined, for example, using $w_{80} = v_{90} - v_{10}$. The absolute assymetry in the line profile A is defined as $((v_{95} - v_{50}) - (v_{50} - v_5))/(v_{95} - v_5)$ (Zakamska and Greene, 2014).

We also define the blueshift of the [O III] emission, which is a measure of the velocity shift of the profile from the expected position. This requires a measure of the observed line position, and an accurate measurement of the quasar systemic redshift. We use v_{10} to mesaure the location of the [O III] emission. Note that v_{50} is not suitable because when [O III] is low S/N we fit with single Gaussian.

The line width measures are not at present corrected for instrumental broadening, but this can easily be done.

1.3.2 *Other flags*

Flag 2

Low S/N. Includes some of the strong iron emitters.

Flag 3

74 objects where [O III] is undetected, although I don't have a rigorous definition of what this means. Merge with 2?

1.4 ICA COMPONENT FITS

What is the segue here? Sometimes Gaussians give poor fit? Not clear what is Hb, what is OIII, what is Fe? Show some examples of when the multi-Gaussian fits fail. Need to describe sample used in ICA component decomposition and briefly describe method (or refer to Allen & Hewett).

1.5 MEASURING THE QUASAR SYSTEMIC REDSHIFT
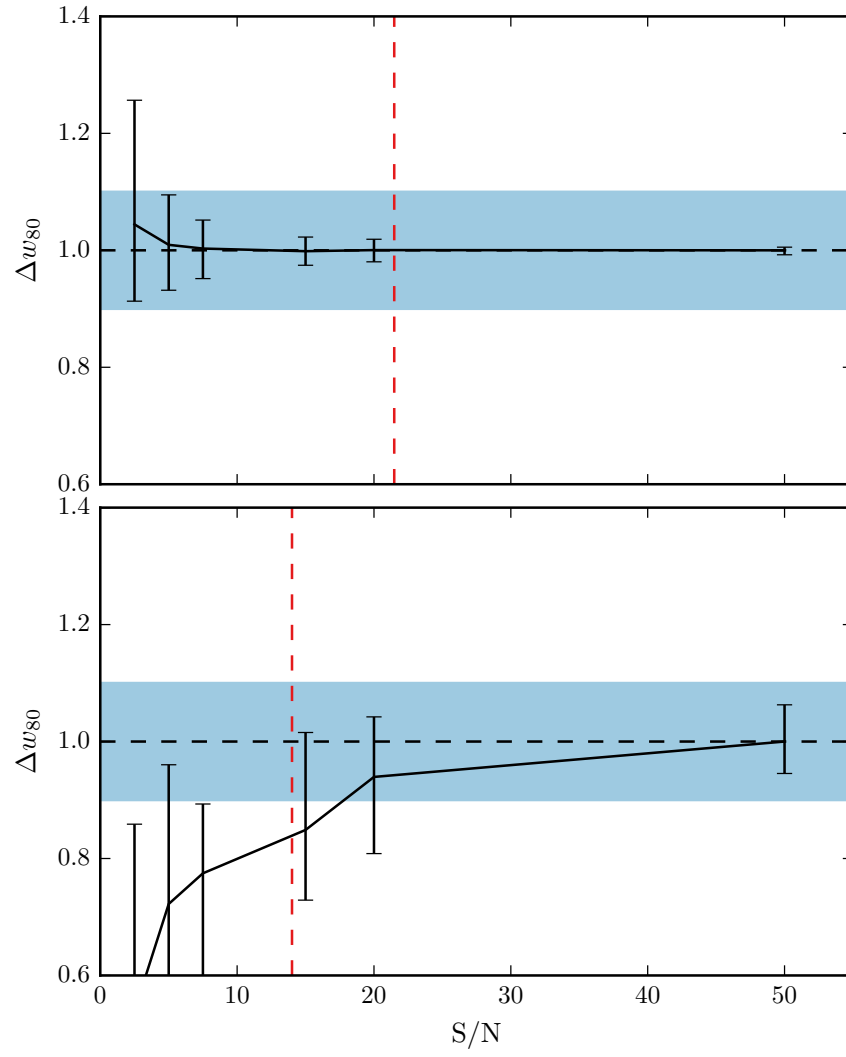
Explain flags Need to send paul redshifts

Figure 1.12

$\mu = -0$
$\sigma = 340$

$c(z_{[\text{OIII}]} - z_{\text{H}\beta})/(1 + z_{[\text{OIII}]})$ [km s^{-1}]

$\mu = -99$
$\sigma = 305$

$c(z_{[\text{OIII}]} - z_{\text{H}\alpha})/(1 + z_{[\text{OIII}]})$ [km s^{-1}]

$\mu = 36$
$\sigma = 217$

$c(z_{\text{H}\beta} - z_{\text{H}\alpha})/(1 + z_{\text{H}\beta})$ [km s^{-1}]
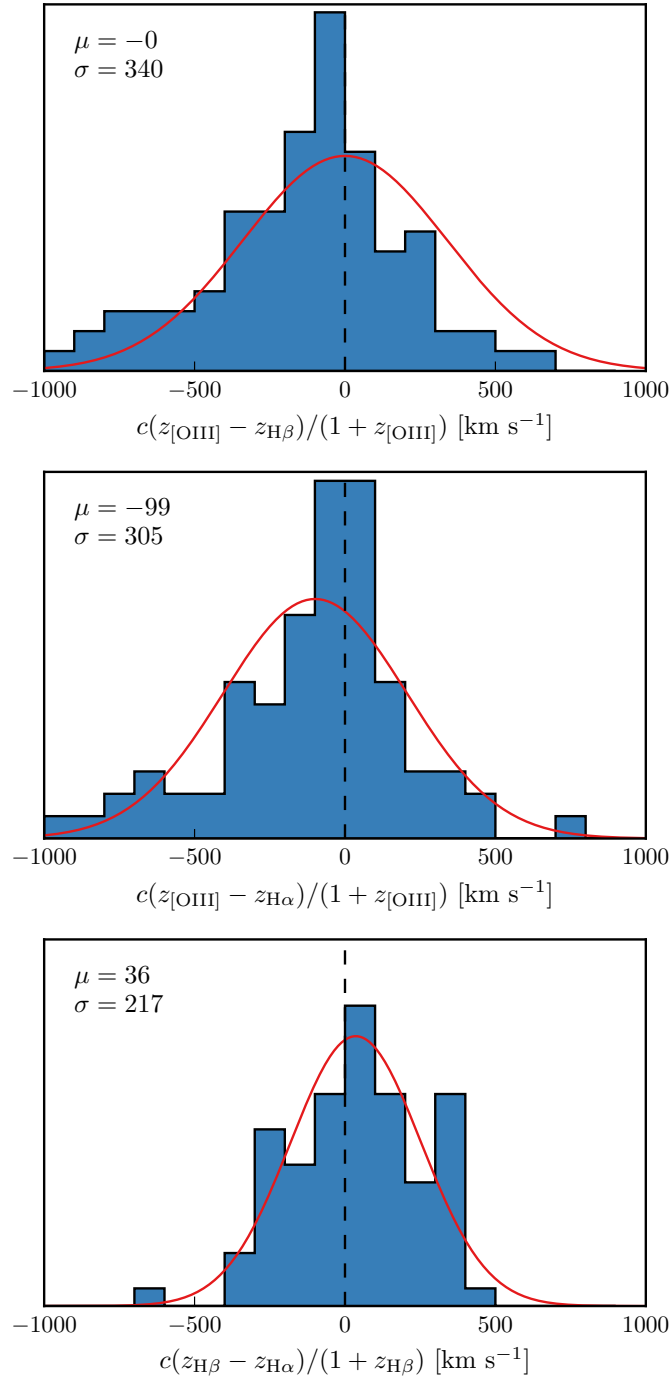
Figure 1.13: Redshift comparisons. Lots have been excluded from Ha/Hb so need to look at flags greater than one. What is the big peak? Gaussian fit to the first one has failed. Find out why these plots look different to ones in paper.

1.5.1 *Hα*

There are 224 quasars in our sample with spectra covering the Hα emission line. We discard seven of these from our sample because of very low S/N (<2.5 measured in the Hα line), leaving 217 To measure the position of the line we fit a parameteric model, which is very similar to the model described in Paper I. The continuum emission is first modeled and subtracted using the procedure described in Paper I. We then test five different models with increasing degrees of freedom to model the Hα emission. The model we select is the simplest model for which the fractional change in the reduced chi-squared from the model with the lowest reduced chi-squared is less than ten per cent.

The models we test are: (1) a single broad Gaussian; (2) two broad Gaussians with identical velocity centroids; (3) two broad Gaussians with different velocity centroids; (4) two broad Gaussians with identical velocity centroids, and additional narrower Gaussians to model the narrow Hα emission, and the narrow components of [N II]$\lambda\lambda$6548,6584 and [S II]$\lambda\lambda$6717,6731; (5) two broad Gaussians with different velocity centroids, and additional narrower Gaussians. If used, the width and velocity of all narrow components are set to be equal in the fit, and the relative flux ratio of the two [N II] components is fixed at the expected value of 2.96. The number of quasars fit by each model is: model 1 - 10; model 2 - 71; model 3 - 32; model 4 - 51; model 5 - 53. The redshift is then measured at the peak flux of the Hα model, including both the broad and narrow components of Hα if appropriate.

1.5.2 *ICA*

The only sensible way to measure the systemic redshift is using the NIR ICA fit. Hα and Hβ seem to give no systematic offset but large scatter, and they are often asymmetric, so should only use peak. And Hα isn't always available, and have other narrow components need to decompose. O III peak is mostly fine to use, but then there are some objects where the whole line is blueshifted. And critically, at large CIV blueshifts the [O III] emission is often undetected. Can show comparison of NIR ICA redshifts to... Optical ICA? Hewett & Wild?

Should emphasise that most people use [O III] to get the most reliable systemic redshift. While this is fine at low luminosities, at high luminosities this can result in large errors (profile can be dominated by blueshifted component, Fe emission can be improperly subtracted, or [O III] might not be detected at all. Publish ICA components with this paper?

Can also describe what I found trying to get redshifts from broad Hα, Hβ? (Narrow components generally very weak at these luminosi-

ties so can't be used.) Generally find no systematic errors but large ($\sim$1000km s^{-1} scatter). Comparing NIR ICA to [O III] for the [O III] with high S/N I find small (few hundred km s^{-1}) scatter.

Should publish [O III] redshifts with this paper for people to use.

1.5.3 *Parameter uncertainties and upper limits*

Describe how uncertainties on best-fitting parameters were calculated.

In 78 quasars, or approximately 25 per cent of or sample, the [O III] is undetected, or detected with very low S/N. In this section we describe how upper limits on the [O III] equivalent width were calculated. Firstly, the best-fitting model comprising the continuum, Fe II, and Hβ emission is subtracted from the spectra, leaving behind only emission due to [O III]. From this spectra we generate 100 mock spectra, where the flux at each wavelength is randomly drawn from a Normal distribution with a mean equal to the flux convolved with a Gaussian of width 200km s^{-1}and a width equal to the known error. We then perform an error-weighted linear least-squares regression with an [O III] template derived from a fit to a very high S/N low redshift SDSS composite spectra. The equivalent width of the best-fitting model is recorded for each of the 100 realisations of the spectra. The error in the equivalent width is defined as the root-mean-square of these values.

Calculated uncertainties using Monte Carlo. Uncertainties on v10 are very large, which I think makes sense since the wing Gaussian will be appearing and disappering, giving a large dispersion in v10. Or regardles v10 is just very sensitive to the noise. Maybe I should be using v25 instead?

1.5.4 *Absolute flux calibration of spectra and continuum luminosities*

Relative flux-calibration of the infrared spectra as a function of wavelength has been achieved, to $\simeq$10 per cent, through observations of appropriate flux standards. The absolute flux levels, however, can be in error by large factors due to variable atmospheric conditions combined with the narrow slit widths. For the majority of the quasars we have, therefore, established the absolute flux scale for each near-infrared spectrum using the same quasar SED-model fitting scheme employed in Paper I. Briefly, the SED-model was fit, with the normalisation and E(B-V) as free varibales, to optical/infrared magnitudes, or SDSS/BOSS spectra (check order I do this.) This allows us to extrapolate from the optical when we do not have photometric data in the near-infrared. The spectra were then normalised to the SED model using a linear error-weighted least-squares regression in the the regions of the spectra covered by the H/K bands. The monochromatic contin-

uum luminosity at 5100Åwas calculated directly from the normalised SED-model. **If this sounds strange can also calculate from fit to normaised spectra. Check if any missing normalisation / monochromatic luminosities.**

1.6 RESULTS FROM ICA FITS

Need to convince the reader that the ICA components approximately correspond to real components. Explain how non-parameteric measures derived form ICA reconstructions.

We find there is a decreasing symmetric component at high luminosities. Relates directly to Shen and Ho, (2014). A stable narrow line region is removed by the outflowing material. Shen and Ho, (2014) showed that the strength of the core [O III] component decreases with quasar luminosity and optical Fe II strength faster than the wing component, leading to overall broader and more blueshifted profiles as luminoisty and Fe II strength (or C IV blueshift) increases.

1.7 LUMINOSITY/REDSHIFT-EVOLUTION OF [O III] PROPERTIES

In this section we look for any luminosity/redshift dependent changes in the [O III] line properties. To do this we extend the dynamic range of our samples in terms of both luminosity and redshift by supplementing our sample with quasars presented by Zakamska and Greene, (2014) and Harrison et al., (2016).

The Zakamska and Greene, (2014) objects are a sample of 568 obscured luminous quasars selected from SDSS (Reyes et al., 2008; Yuan, Strauss, and Zakamska, 2016). They are selected to have [O III] luminosities above $10^{8.5} L_\odot$ and have a median redshift $z = 0.397$.

We also include 40 quasars at redshifts $1.1 \leqslant z \leqslant 1.7$) from the KMOS AGN Survey at High redshift (KASHz) with [O III] line measurements.

We also have the same information for ~20 000 SDSS spectra from Mullaney et al., (2013).

In Figure 1.14 we show the [O III] velocity width as a function of the [O III] luminosity and the quasar redshift. The lack of any redshift-evolution between $z = 0$ and $z = 1.5$ was reported by Harrison et al., (2016). Our additional data suggests that this continues to $z \sim 2.5$. On the other hand, at fixed redshift, we see a significant correlation between the [O III] velocity width and the luminosity.

The fact that we don't see many broad lines in the Zakamska and Greene, (2014) objects even at luminosities >43 erg/s could be due to the fact that these are all type II quasars, whereas the sample presented in this paper are all type I. Mullaney et al., (2013) showed that the [O III] lines of type I quasars are typically broader than in type II quasars.
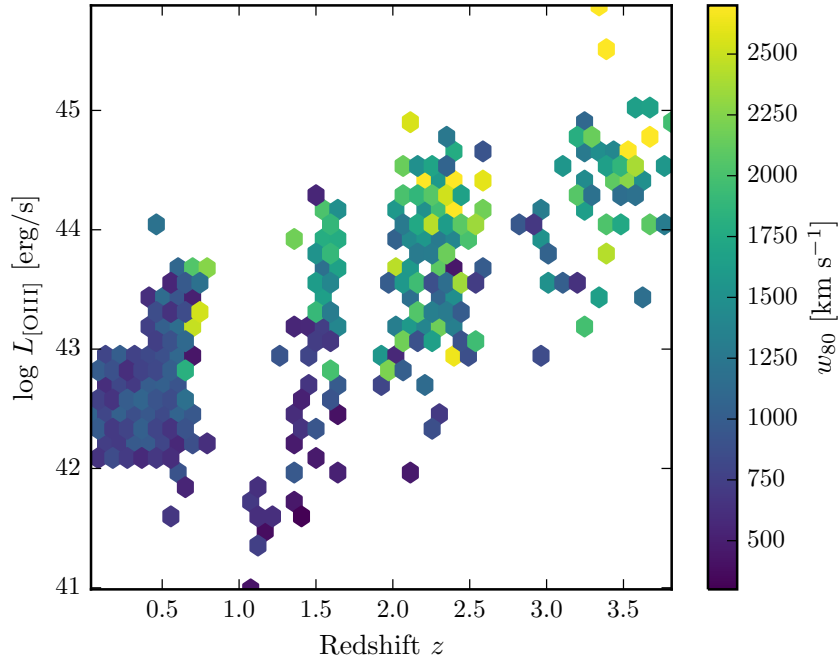
Figure 1.14: The [O III] velocity-width, characterised by w_{80}, as a function the [O III] luminosity and the quasar redshift. The color of each hexagon denotes the mean w_{80} for the obects in that luminosity-redshift bin. We have suplemented our sample with low-z objects from Zakamska and Greene, (2014) and medium ($z \sim 1.5$) redshift objects from Harrison et al., (2016). If I keep this plot make sure its clear which points belong to which sample.
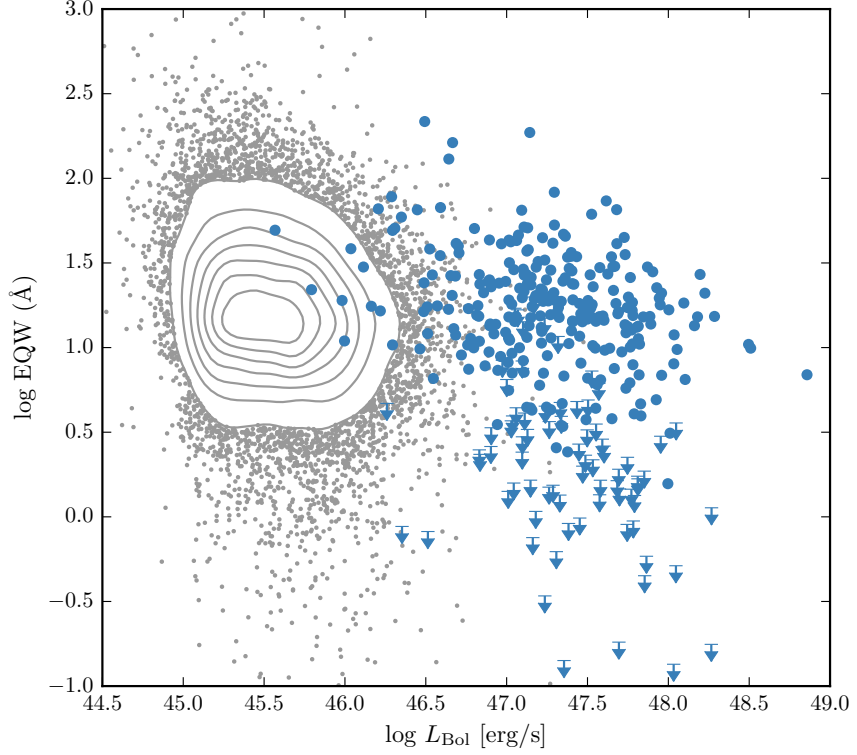
Figure 1.15: The [O III] EW as a function of the quasar bolometric luminosity for the sample presented in this paper (blue circles) and the low-z SDSS sample (grey points and contours). Upper limits are denoted by the downward arrows.

Looking at the [O III] velocity width as a function of luminosity tells us about the physical drivers of the outflows observed in [O III]. The correlation with luminosity suggests that the highest velocity outflows are associated with the most luminous AGN. This has been reported for low-redshift AGN, for both ionized and molecular outflows (e.g. Westmoquette et al. 2012; Veilleux et al. 2013; Arribas et al. 2014; Cicone et al. 2014; Hill & Zakamska 2014).

This suggests that the outflows are driven by radiative forces. On the other hand, Mullaney et al., (2013) find that once the correlation between the [O III] luminosity and the radio luminosity has been taken in to account, the [O III] velocity width is more strongly related to the radio luminosity of the AGN.

1.8 EQUIVALENT WIDTH

In Fig. 1.15 we show the [O III]5008 EW as a function of the quasar bolometric luminosity. Bolometric luminosity is estimated from the monochromatic continuum luminoisty at 5100Åusing the correction

factor given by Richards et al., (2006). For comparison, we also show the low-z sample from Shen et al., (2011).

The equivalent width of [O III] has been found to strongly decrease as a function of redshift and/or luminosity (e.g. Brotherton, 1996; Netzer et al., 2004; Sulentic et al., 2004; Baskin and Laor, 2005).

The size of the narrow line region is roughly expected to scale as $L^{0.5}$ (e.g. Netzer et al., 2004). However, for high luminosity quasars with strong [O III] this gives NLR sizes which are unreasonably large (~100 kpc; Netzer et al., 2004).

Netzer et al., (2004) found 1/3 of their high luminosity sample had very weak [O III], whereas quasars with weak [O III] are very rare for nearby AGN. We find a very similar fraction. Netzer et al., (2004) claim that for the population of strong [O III] emitters there is no reduction of EW with increasing source luminosity. On the other hand, there are many weak or no [O III] emitters at high luminosity that could give the impression that the line EQW decreases with increasing source luminoisity.

1.8.1 *OIII outflows*

Our best-fitting profiles show a strongly blue-asymmetric profile (Fig. 1.16), with a significant fraction of the total emission in a blue wing. The luminous blueshifted broad wing and the exteremely broad profile reveals high-velocity outflowing ionized gas. This can be explained if the far-side of any outflowing gas, that is moving away from the line of sight, is obscured by dust in the host galaxies (e.g. Heckman et al. 1981; Vrtilek 1985). Observations at both low and high redshifts commonly observe this blueshifted component. Our results, and those of other authors, suggest that kpc-scale outflows in ionized gas are common among the most luminous high-redshift actively accreting SMBHs.

The situtation is very different in nearby AGN, where the [O III] velocity width is dominated by the galactic potential and correlates well with the stellar velocity dispersion. HI, CO and absorption line mesaures of the host galaxy rest frame suggest that [O III] usually gives consistent results within 200 km/s (de Robertis 1985; Whittle 1985; Wilson & Heckman 1985; Condon et al. 1985; Stripe 1990; Alloin et al. 1992; Evans et al. 2001).

We see a correlation between the [O III] velocity width and blueshift. As the blueshift of the line increases it gets broader. This is consistent with Shen and Ho, (2014), where the strength of the narrow core is decreasing, leading to a broader and more blueshifted profile.
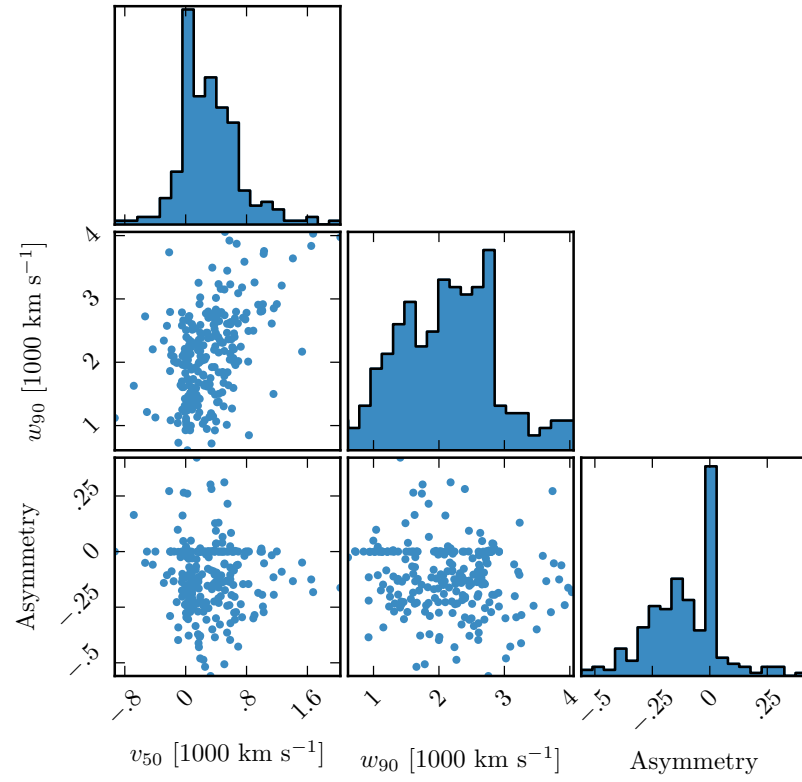
Figure 1.16: The distributions of and correlations between a subset of the non-parameteric measures we made of the best-fitting [O III] models.
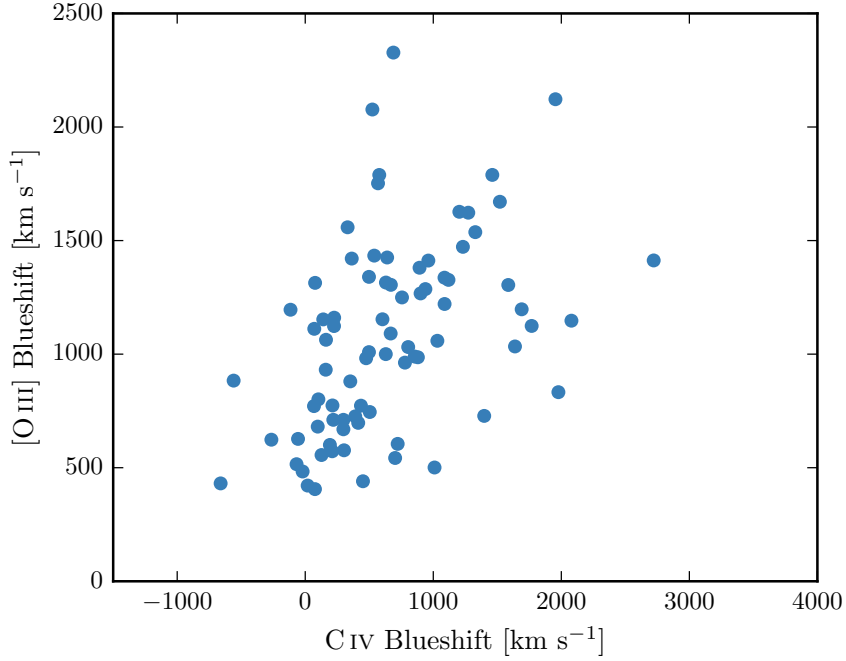
Figure 1.17: The relation between the blueshifts of C ιν and [O ιιι]. Equivalent to Fig 8. We use the Hβ peak in this figure, which I think is responsible for some of the trend. However, we do see a correlation (albeit noisier) using the NIR ICA redshifts. Not a sensible to use the [O ιιι] redshifts, since these become much more unreliable at the high C ιν blueshift end (when [O ιιι] is weaker: figure 7. Note that we are using v_{10} for the [O ιιι] position and v_{50} for the C ιν position. We can't use v_{50} for [O ιιι] because sometimes we are using a single Gaussian, especially if the [O ιιι] is weaker and we miss the broad component. Need to remake this plot / don't use at all because I don't believe some of the Gaussian fits to [O ιιι], especially at high C ιν blueshifts when [O ιιι] is weak and Fe ιι is strong.) Only objects where fit with two components.
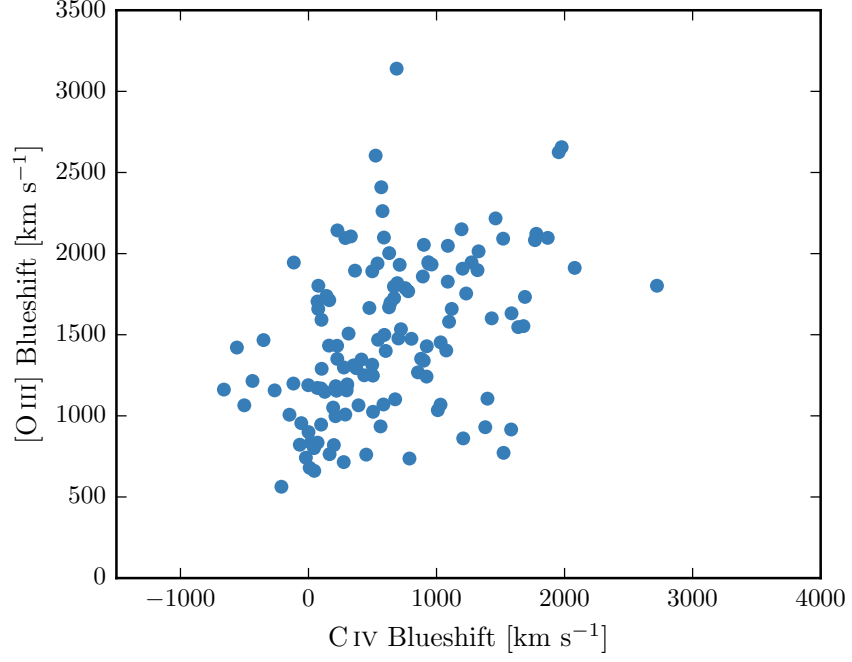
Figure 1.18

1.8.2 *[O III] and C IV outflows are linked*

As described in Paper I, we have searched for optical counterparts to our near-infrared spectra. Optical spectra are available for XXX quasars in our catalogue, and cover the broad C IV doublet. As we described in Paper I and Coatman et al., (2016), C IV is often blueshifted, which almost certainly signal the presence of strong outflows, most likely originating in a disc wind. In Paper I we demonstrated that the quasars in our sample cover the full range of C IV blueshifts seen in the SDSS quasar population, which makes our sample unique in that it allows us to study properties of the quasar across the full parameter range.

The C IV velocity centroid measurements are taken directly from paper I. We define the 'location' of the [O III] emission using v_{10}, although the results are the same if v_{20}, v_{50} etc. are used instead.

In Figure 1.17 we show the C IV blueshifts against the [O III] blueshifts. This comparison is done for a sub-sample of 146 objects where we have good measurements of the C IV, [O III], and Hβ (to measure the systemic redshift) profiles. Objects with S/N > 3 are shown as blue filled circles and objects with S/N < 3 as open grey circles. We calculated the median S/N per pixel in the best-fitting model for the [O III]5008 emission.

There is a clear and strong correlation. Similar correlations have been tentatively found in lower redshift quasars and AGN (Zamanov et al., 2002).
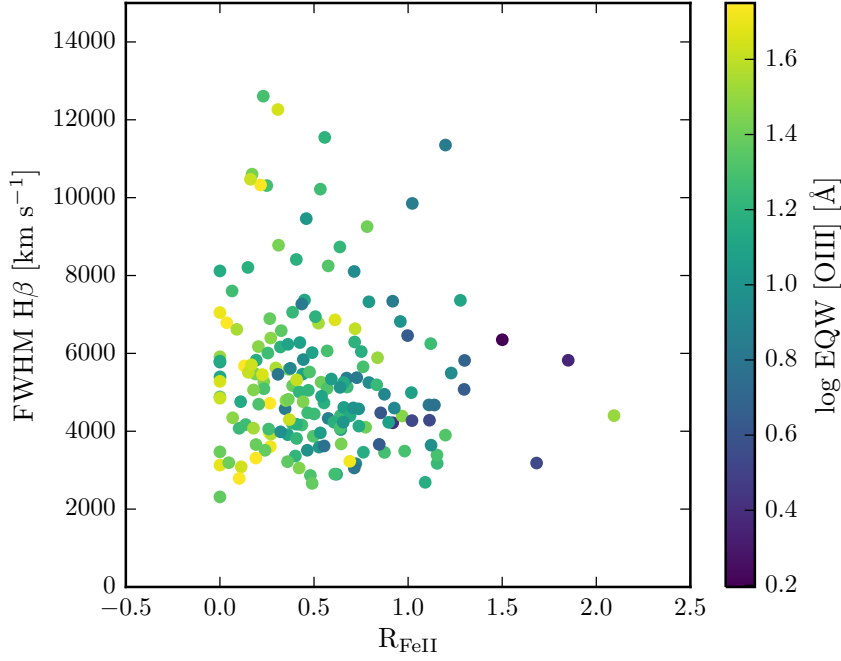
Figure 1.19: The [O III] EQW as a function of the Hβ FWHM and the optical Fe II strength (EQW Fe II/ EQW Hβ).

The blueshifting of C IV is known to correlate with luminosity (Richards et al., 2011). In [O III], the blueshifted wing becomes relatively more prominent as the luminosity of the quasar increases (Shen and Ho, 2014). Therefore, it is plausible that the correlation between the C IV and [O III] blueshifts is a secondary effect that is driven by the correlation of each with the luminosity. In Figure **??** we color the data points by the luminosity, and no luminosity-dependent trends are apparent. We find that both the [O III] and C IV blueshifts are correlated with the luminosity, but that these correlations are much weaker than the correlation between the [O III] and C IV blueshifts.

1.9 EIGENVECTOR ONE CORRELATIONS

In Figure 1.19 we show the [O III] EQW as a function of the Hβ FWHM and the optical Fe II strength. The optical Fe II strength is defined as the ratio of the Fe II and Hβ EQW, where the Fe II EQW is measured between 4434 and 4684Å. These parameters form part of 'eigenvector 1' (EV1), the first eigenvector in a principal component analysis which originated from the work of Boroson and Green, (1992). In our sample, these parameters follow very similar correlations to what is observed at low-z (e.g. Shen and Ho, 2014). In particular, the anti-correlation between the [O III] and Fe II EQWs.
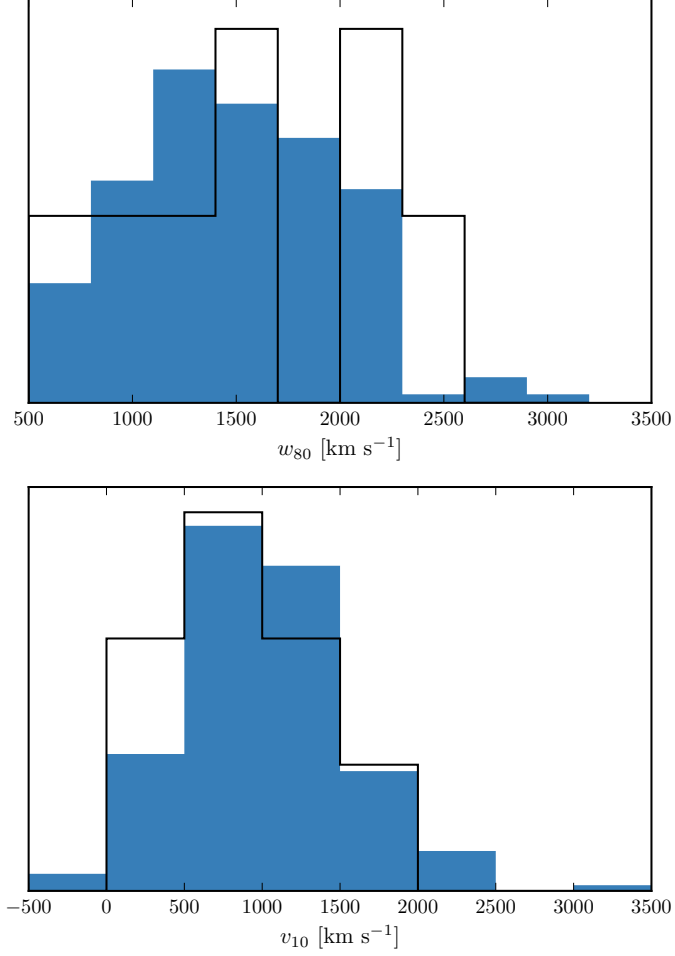
Figure 1.20: The distribution of w_{80} and v_{10} for the 19 BALs are compared to the distribution for the non-BALs. These look rubbish. Cumulative distributions instead? Try doing gaussian kernel density estimator

Same as Shen, (2016), we confirm that the EV1 correlations hold at high luminosities/redshifts. See also Sulentic et al. 2004, 2006; Runnoe et al. 2013. Make sure it's clear that Shen, (2016) quasars make up a significant chunk of our sample.

1.10 MAPPING EV1 TO CIV BLUESHIFT AND EQW

1.11 SIGNAL TO NOISE TESTS

1.12 BROAD ABSORPTION LINE QUASARS

19 quasars in our catalogue are classified as broad absorption line (BAL) quasars, using the either the SDSS classification flags or the Allen et al., (2011) catalogue. We find that the BAL quasars have typ-

ically broader [O III] than the rest of the sample. Note that in the Zakamska et al., (2016) sample of very red quasars, the incidence of BALs is very high, and these objects have extremely broad [O III] profiles. A two-sided Kolmogorov-Smirnov statistic on the w_{80} distributions returned a p-value of 0.10. What does this mean? Try with different parameters? Histograms look rubbish so maybe just give the numbers.

1.13 DISCUSSION

1.13.1 *Type II quasars*

Implications of our findings on searches for high-redshift type 2 quasars. It could be that type II quasars exist. If you look at CIV/MgII the narrow line components are very weak. So the contribution from the narrow line region is very weak in luminous quasars, and you just won't see it even if the broad line region is obscured. Findings in this paper seem to suggest that the startic narrow line region is very weak in luminous quasars.